Journal of Physics and Chemistry of Solids 128 (2019) 237–244

Contents lists available at ScienceDirect

Journal of Physics and Chemistry of Solids

journal homepage: www.elsevier.com/locate/jpcs

# Spin-resolved electronic structure of ferroelectric α-GeTe and multiferroic $Ge_{1-x}Mn_xTe$

J. Krempaský [a,*], M. Fanciulli [a,b], N. Pilet [a], J. Minár [c], W. Khan [c], M. Muntwiler [a], F. Bertran [d], S. Muff [a,b], A.P. Weber [a,b], V.N. Strocov [a], V.V. Volobuiev [e,f], G. Springholz [f], J.H. Dil [a,b]

[a] Swiss Light Source, Paul Scherrer Institut, CH-5232 Villigen PSI, Switzerland
[b] Institute of Physics, École Polytechnique Fédérale de Lausanne, CH-1015 Lausanne, Switzerland
[c] New Technologies-Research Center University of West Bohemia, Plzeň, Czech Republic
[d] SOLEIL Synchrotron, L'Orme des Merisiers, F-91192 Gif-sur-Yvette, France
[e] National Technical University, Kharkiv Polytechnic Institute, Frunze Str. 21, 61002 Kharkiv, Ukraine
[f] Institut für Halbleiter-und Festkörperphysik, Johannes Kepler Universität, A-4040 Linz, Austria

A B S T R A C T

Germanium telluride features special spin-electric effects originating from spin-orbit coupling and symmetry breaking by the ferroelectric lattice polarization, which opens up many prospectives for electrically tunable and switchable spin electronic devices. By Mn doping of the α-GeTe host lattice, the system becomes a multiferroic semiconductor possessing magnetoelectric properties in which the electric polarization, magnetization and spin texture are coupled to each other. Employing spin- and angle-resolved photoemission spectroscopy in bulk- and surface-sensitive energy ranges and by varying dipole transition matrix elements, we disentangle the bulk, surface and surface-resonance states of the electronic structure and determine the spin textures for selected parameters. From our results we derive a comprehensive model of the α-GeTe surface electronic structure which fits to experimental data and first principle theoretical predictions and we discuss the unconventional evolution of the Rashba-type spin splitting upon manipulation by external B- and E-fields.

## 1. Introduction

Whenever the structural inversion symmetry is broken, spin-orbit coupling (SOC) lifts the spin degeneracy of states according to the so-called Rashba effect [1]. Rashba-type effects were first observed in quantum confined two-dimensional electronic states in semiconductor heterostructures due to the artificial structural asymmetry created at the interfaces [2,3]. The Rashba splitting of these electronic states can be tuned electrically but the splitting is rather small, limiting practical device applications. On heavy metal surfaces [4–10], in metallic quantum well states with enhanced SOC [11–13], and on surfaces of topological insulators [14] and transition metal oxides [15] much larger splittings were found. The additional advantage is that such states are directly accessible by spin- and angle-resolved photoemission spectroscopy (SARPES) [16,17]. A three-dimensional (3D) form of the Rashba-effect was found in a series of bismuth tellurohalides BiTe$X$ $X$ = I, Br, or Cl [18–23]. Although these materials exhibit a very large spin-splitting they lack an important property concerning functionalisation, namely, the possibility to switch or tune the spin texture. This limitation can be overcome in a new class of functional materials displaying Rashba-splitting due to ferroelectricity.

In ferroelectrics the large natural structural asymmetry due to the ferroelectric (FE) lattice displacements leads to a large Rashba splitting even of the bulk bands for which reason such materials have been named ferroelectric Rashba semiconductors (FERS) [24]. The most prominent example is α-GeTe featuring a record spin splitting and Rashba parameter [25]. From the technological point of view GeTe also belongs to a class of chalcogenide phase-change materials [26,27] and it is the ferroelectric semiconductor with the simplest conceivable binary structure [28,29] with strongly asymmetric arrangement of the Ge and Te atoms along the ⟨111⟩ direction [25].

Recently, α-GeTe has attracted a flurry of experimental activity [25,30–34] because of its giant Rashba effect, theoretically predicted by S. Picozzi et al. [24,35]. The highly non-centrosymmetric arrangement of the Ge and Te atoms along the ⟨111⟩ direction combined with the large spin-orbit coupling is at the heart of this effect, resulting in the highest reported bulk Rashba coupling parameter $\alpha_R$ of 4.25 eVÅ [25]. The theoretical Rashba concept proposed in Ref. [24] was further refined by semi-infinite crystal calculations to address the canted spin arrangement as observed in SARPES [25].

* Corresponding author.
*E-mail address:* juraj.krempasky@psi.ch (J. Krempaský).

https://doi.org/10.1016/j.jpcs.2017.11.010
Received 8 August 2017; Received in revised form 29 October 2017; Accepted 7 November 2017
Available online 8 November 2017

Doping of GeTe with Mn induces additional ferromagnetic (FM) order leading to multiferroicity in $Ge_{1-x}Mn_xTe$ already for moderate Mn doping levels [31], similar to the two-dimensional electron gas on the surface of $SrTiO_3$ [15] and the surface states of vanadium-doped BiTeI [36]. Because the magnetization direction is perpendicular to the surface, this opens an additional band gap at the zone center in the Rashba-split bulk states. This moreover leads to a vertical spin polarization at the Z-point of the Brillouin zone (Fig. 1b) that can be switched by reversal of the magnetization, as revealed by SARPES data from magnetized samples [31]. The ferroelectricity is induced by the lattice distortion of GeTe and ferromagnetism by the coupling of the local spins of the Mn ions via the free carriers in system [37]. Fig. 1 summarize the $Ge_{1-x}Mn_xTe$ thin film basic properties in terms of atomic arrangement (panel a), bulk and surface Brillouin zone (b), ferromagnetic hysteresis (c), surface topography (d) and ferroelectric response measured in piezo-force microscopy (e). Due to high Mn solubility and high hole concentration, the magnetic transition temperature of $T_C = 190$ K is amongst the highest of all FM semiconductors. This new class of materials, termed multiferroic Rashba semiconductors (MUFERS), also displays a new type of magnetoelectric coupling due to entangled Rashba and Zeeman effects [31].

Nonetheless, this overwhelming panel of physical properties might also hide unconventional pairings because the system naturally possesses bulk type-II superconductivity in a non-centrosymmetric lattice arrangement [38,39]. For this reason further experimental effort is made to engineer topologically non-trivial systems based on $Ge_{1-x}Mn_xTe$ by adequate doping in order to optimize material conditions for hosting 'Majorana'-like quasiparticles [40].

In this paper, we present a comprehensive review of the α-GeTe and $Ge_{1-x}Mn_xTe$ surface electronic structure studied by (spin- and) angle-resolved photoemission ((S)ARPES). Experiments were performed on 200 nm thick films grown by molecular beam epitaxy on $BaF_2$(111) substrates [37,41,42]. A protective stack of amorphous Te- and Se-capping layers with a total thickness of 20 nm was used to avoid surface oxidation and degradation. This cap was completely removed in the ultrahigh vacuum ARPES chamber by annealing the samples for a total of 30 min at 250 °C.

The spectra are discussed in detail in comparison with results from *ab-initio* calculations based on the multiple scattering approach in density functional theory [43]. Spin-orbit coupling has been naturally included by use of a fully relativistic four-component scheme. As a first step of our investigations we performed self-consistent calculations for 3D bulk as well as 2D semi-infinite surface of α-GeTe within the screened Korringa-Kohn-Rostoker formalism [43]. The corresponding ground state band structures are presented in terms of Bloch spectral functions. These self-consistent results served as an input for our spectroscopic investigations. The ARPES calculations were performed in the framework of the fully relativistic one-step model of photoemission in its spin-density matrix formulation, which accounts properly for the complete spin-polarization vector, in particular for Rashba systems like α-GeTe.

The first issue we address is to show that α-GeTe is a narrow gap semiconductor in which the bulk bands, buried inside the α-GeTe surface electronic structure probed by ARPES, do not reach the Fermi level in contrast to what was recently claimed [30]. Because there is a conspicuous difference in the ARPES interpretation in this respect, we here demonstrate that pure surface and bulk states can be clearly distinguished in ARPES and that the surface and bulk Dirac points are well separated in energy. Since surface effects are quenched on capped α-GeTe surfaces [25], a direct inspection of bulk states is possible, proving that α-GeTe is a ferroelectric Rashba semiconductor with a band gap of about 60 meV. On the other hand, for uncapped surfaces the bulk band edges are difficult to observe due to the presence of strong surface resonance states. This is especially the case near the Z-point where the band gap is smallest and the Rashba splitting is most pronounced [24,25].

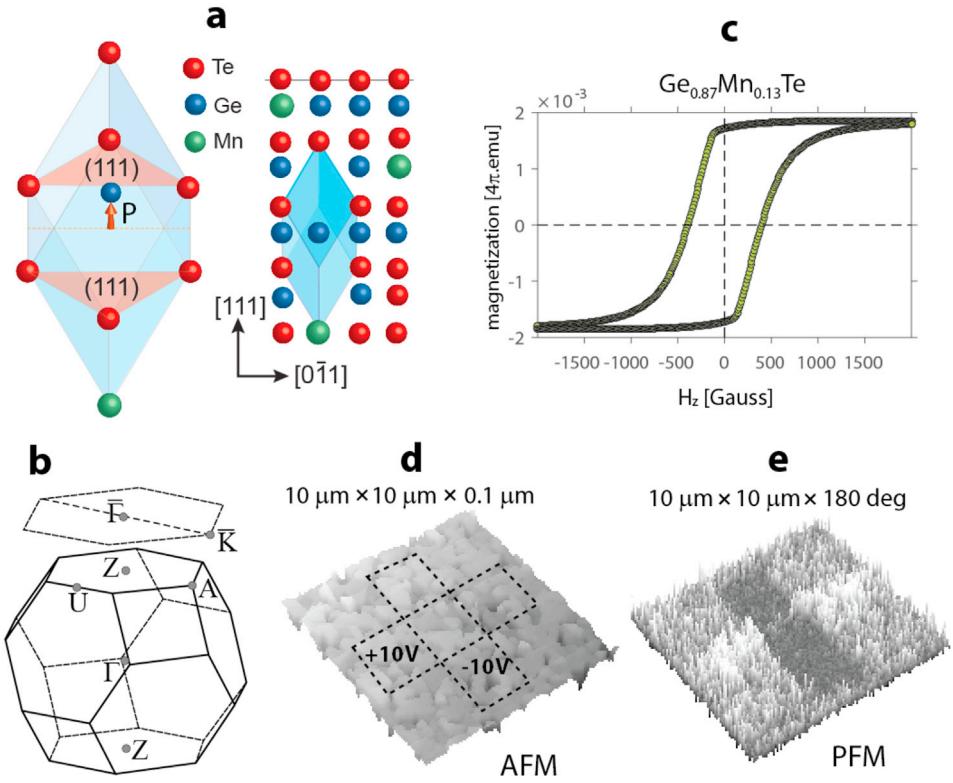


**Fig. 1.** (a) Sketch of multiferroic $Ge_{1-x}Mn_xTe$ with ferroelectric displacement of Ge(Mn)-atoms inside the rhombohedrally distorted unit cell along [111] as indicated by the orange arrow. Blue shading indicates the α-GeTe rhombohedral unit cell, the red shadings indicate the (111) Miller planes. (b) The Brillouin zone of rhombohedrally distorted (quasicubic) GeTe. (c) Out-of-plane ferromagnetic hysteresis curve of multiferroic $Ge_{0.87}Mn_{0.13}Te$ measured by SQUID. (d) Surface topography measured in atomic force microscopy (AFM). (e) Piezo-force microscopy (PFM) showing 180 ° phase change in writing two domains with ±10 V forming a cross (dashed rectangles in d). The experimental setup is measuring AFM and PFM data from $Ge_{0.87}Mn_{0.13}Te$ simultaneously. (For interpretation of the references to colour in this figure legend, the reader is referred to the web version of this article.)

## 2. α-GeTe surface electronic structure

To distinguish the surface electronic structure of α-GeTe we compare in Fig. 2 ARPES data measured near Z-points with different photon energies of 22, 70 and 480 eV at the COPHEE [44], Pearl [45] and ADDRESS [46] photoemission experimental stations at the Swiss Light Source, respectively. All data were measured at or below 35 K. For each photon energy, constant energy cuts at a given binding energy (isosurfaces) are compared. The isosurfaces at the Z-point in panels a,d and f of Fig. 2 have six-fold symmetry, whereas away from the Z-points the isosurfaces assume a three-fold symmetry as indicated by dashed lines in the bottom panels of (c,d). The schematic picture in Fig. 3a illustrates how the 6-fold symmetry at the Z-point changes to three-fold above $(Z+\Delta)$ and below $(Z-\Delta)$ the Z-point, by showing the top-view of the distorted spindle-torus 3D constant energy surface of α-GeTe [25].

The ARPES data in Fig. 2 shows the influence of the photoelectron escape depth when probing the same electronic structure in surface sensitive vacuum ultraviolet ($h\nu = 22$ or 70 eV) and more bulk sensitive soft-X ray ($h\nu = 480$ eV) [47]. This comparison allows us to identify the surface states (SS), bulk states and the elusive surface resonances (SR). As extensively discussed in Ref. [25], disentangling the SR and bulk bands for α-GeTe near the Z-point is challenging because in the vicinity of the Z-point the SR bands show much higher spectral weight compared to the bulk states. Moreover, they disperse with photon energy and are thus easily confused with bulk states [30]. Therefore in ARPES one observes metallic states at $E_F$, in general agreement with the intrinsic *p*-type doping from Ge vacancies responsible for the metallic character of the nominally semiconducting GeTe [48]. However, tunnelling experiments provide firm experimental evidence that α-GeTe is a narrow-gap semiconductor [28]. This gap of around 60 meV can also be seen in Fig. 2b buried below the surface electronic structure. The band map clearly resolves the narrow-gapped bulk states (black dashed lines) and their surface resonance-replica (red dashed lines) shadowing the bulk states and shifted up to $E_F$.

Generally speaking, in photoemission experiments the observation of SR bands is expected to occur around the edge of the projected bulk band structure of semiconductors [49–51]. In this sense, α-GeTe is a textbook example and ignoring the relevance of the SR bands can lead to an erroneous interpretation of the surface electronic structure. This underlines again the importance to combine bulk and surface sensitive photoemission. The data in Fig. 2 reveals the SR-bands detaching from pure surface states in panel (a), progressively enhancing their spectral weight for lower binding energies by forming a 30 ° rotated isosurface compared to pure surface states. The spectral weight of these surface states near the Z-point at $h\nu = 70$ eV piles up at the extremities of the hexagonally-warped bulk states (panels *c*–d), and for the Z-point probed with $h\nu = 480$ eV in panel (f) their spectral weight vanishes because of the increased bulk sensitivity.

Projecting all the isosurfaces from surface- and bulk-sensitive ARPES on a single plane we see the SR bands detaching from the pure surface states and hybridizing with the bulk continuum, as schematically depicted in Fig. 3b in red. The momenta at selected binding energies where the intensity is increased due to hybridization of SR and SS states (yellow markers in Fig. 3d) are overlaid with first-principles calculations to show that along the mirror planes (in this case along $\overline{\Gamma K \Gamma}$), the surface resonances follow the dispersion of the two major surface states denoted $S_1$ and $S_2$. We readily see that these surface states have their Dirac point in the unoccupied states because they do not fold back below $E_F$, and are well separated from the bulk states. In Fig. 2c we observe that SR bands outside the Z-point disperse along the bulk bands by changing the isosurfaces from six to three-fold symmetry, which illustrates how the SR bands mimic the bulk bands, and at the same time, in mirror planes they

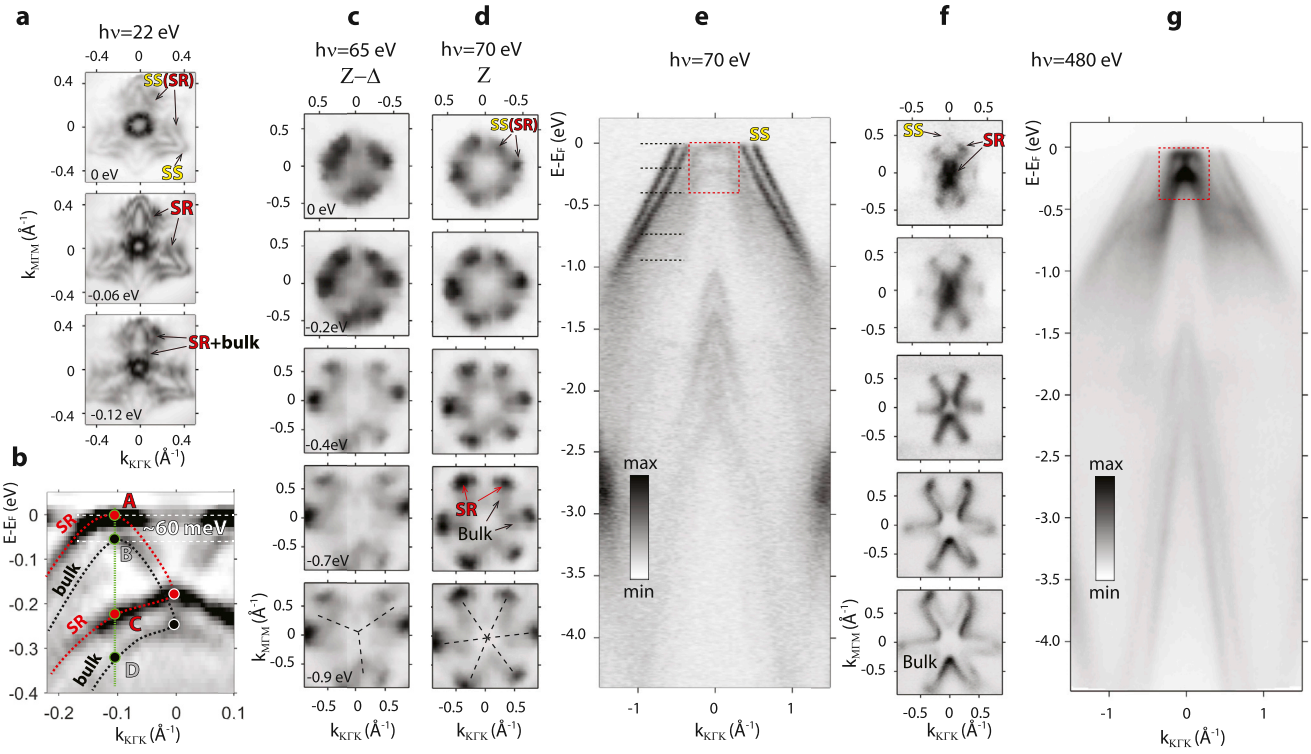


**Fig. 2.** ARPES band maps and isosurfaces near the Z-point of α-GeTe measured at different photon energies: (a,b) $h\nu = 22$ eV; (c–e) 65 and 70 eV; (f,g) 480 eV. ARPES data were measured with *p*-type light polarization. The isoenergy surfaces (isosurfaces) in panels (c,d,f) were measured at binding energies indicated in panel (e) by horizontal dashed lines. Note that the data in (c,d) was obtained with a 50 times lower statistics as in (e). The arrows indicate momenta for pure surface states (SS) and surface resonances (SR) with respect to bulk bands, also indicated in red dashed rectangles in (e) and (g). Panel (b) is a second derivative band map with bulk bands shadowed by their resonance replica, vertical green line indicate an EDC-cut intersecting the bands in points A-B-C-D. Dashed lines in bottom panels *c*–d indicate the three-to six-fold isosurface symmetry change. (For interpretation of the references to colour in this figure legend, the reader is referred to the web version of this article.)

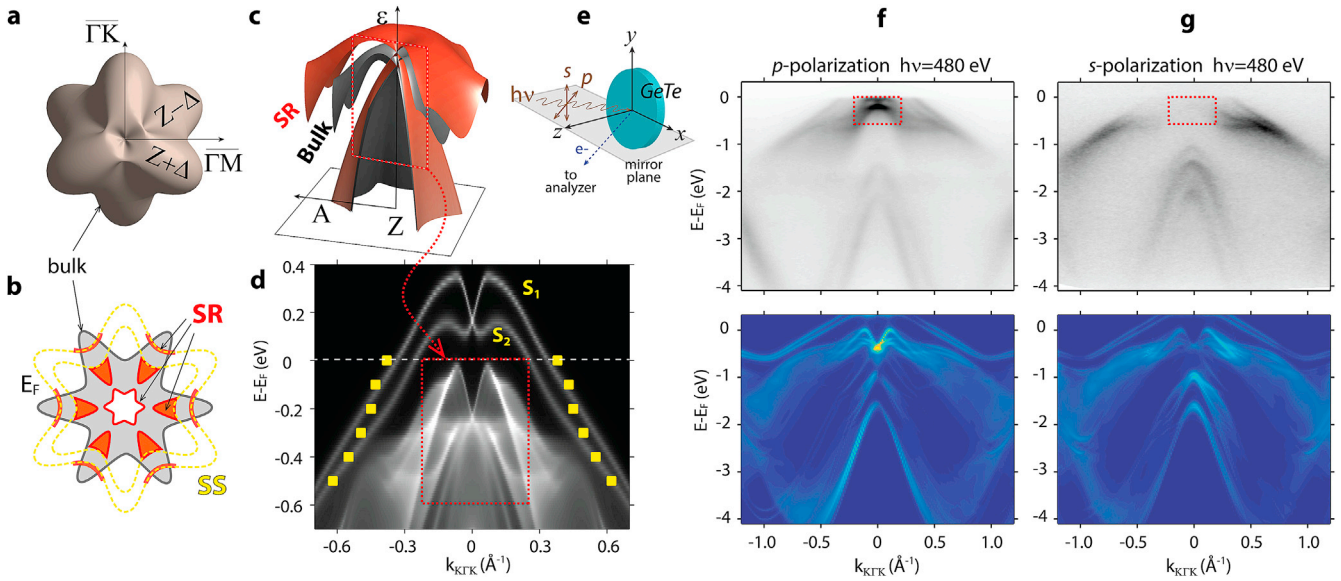


**Fig. 3.** (a) 3D schematic representation of the α-GeTe bulk isoenergy surface at the Z-point and its vicinity (Z±Δ). (b) Schematic projection of the α-GeTe electronic structure onto the surface Brillouin zone; (c) corresponding model of the bulk (black) and bulk-derived SR bands (red). (d) α-GeTe semi-infinite crystal calculations, yellow markers indicate the high intensity spots from Fig. 2 (c,d). (e) Experimental geometry with *p*-polarized light. (f,g) ARPES band maps along $\overline{\text{KΓK}}$ measured with *p* and *s*-polarized light, respectively. Red frame indicate the energy and momenta with bulk properties, bottom panels are calculations. (For interpretation of the references to colour in this figure legend, the reader is referred to the web version of this article.)

mimic the surface states. Such observation is typical to surface resonances which materialize in the sample sub-surface region comparable with the photoelectron escape depth (5-10 Å).

Another approach to reveal the dispersive character of the SR-bands in α-GeTe is a $k_z$ -dispersion movie in the $\overline{\text{KΓK}}$ mirror plane (see Article Enrichment material). The scan stretches over two Z-points in the 3D Brillouin zone and it shows that upon band-gap opening the SR-band separates from the bulk Rashba band and near the maximum gap at the Γ point ($h\nu \approx 400$ eV) it disappears. As the gap is narrowing again in the $k_z$-scan, they reappear and disperse side-by-side with the bulk bands toward $E_F$ such that at the Z-point they can be resolved only in a second derivative of the measured band map (Fig. 2b).

Supplementary data related to this article can be found online at https://doi.org/10.1016/j.jpcs.2017.11.010.

From a technological point of view the pure surface Rashba bands $S_{1,2}$ and their resonances are less important because, as already mentioned, on capped α-GeTe surfaces they are completely quenched. Interestingly, their spectral signatures are also easily explored by variation of transition matrix elements. As shown in Fig. 3f and g, the *p*- and *s*-polarized light, for the experimental geometry depicted in Fig. 3e, almost toggles on and off the bulk and bulk-derived bands. This suggests that the dipole selection rules can be used to select the states originating in Ge and Te $p_z$-orbitals, oriented perpendicular to the sample surface along the ⟨111⟩ direction. This is also confirmed by our one-step photoemission calculations on the bottom panels of Fig. 3f,g.

For a practical description of the α-GeTe bulk electronic structure in surface-sensitive ARPES, Fig. 3b,c shows a simple cartoon view of the bulk and bulk-derived SR bands depicted in black and red, respectively. Until new detection schemes in SARPES become available in the soft X-ray regime capable to investigate pure bulk states [47,52], α-GeTe SARPES data will always integrate the spectral intensity from both the SR and bulk bands.

## 3. Experiments versus first-principles calculations

To illustrate the validity of our electronic structure model, we compare rigorous first principles calculations to the experimental data. Fig. 4 summarizes SARPES data measured in the $\overline{\text{KΓK}}$ mirror plane near the Fermi level (MDC-A) and around a binding energy of 0.5 eV (MDC-B), denoted by dashed frames in Fig. 4d. SARPES data for MDC-A (panel a) and MDC-B (panels b,e) clearly show that the spin texture at higher binding energy is more complex, in agreement with SARPES data measured with a time-of-flight momentum microscope equipped with an imaging spin filter [32].

We note that the appearance of individual peaks is well accounted for in both experiment and theory for both data sets. As seen in Fig. 4b, the more complex MDC-B spin texture is comprehensively described using a 3D vectorial analysis [9,25,53] which fits total intensity and measured 3D spin polarizations (orange lines in Fig. 4b,e, respectively). The {x,y}-projected spin vectors from individual peaks are shown in Fig. 4a,b. Consistent with the calculated spin-resolved band-map in panel (c), the main in-plane spin polarization is detected along the x-direction. Along that direction there are two prominent spin directions indicated by the red and blue arrows in panel (e). Their corresponding vectors are reproduced in panel (b), the remaining spin modulations with minor contributions to the measured spin currents are indicated by black arrows. These two states are the two main bulk-derived Rashba bands, which is evidenced by their antiparallel $P_{x,y}$ spin vector alignment. We note that the spin-switching of these two bands was extensively tested in *operando* SARPES in field effect devices to show that their manipulation by E-fields is possible [33].

The experimental observations in Fig. 4 give us confidence that the highly modulated α-GeTe spin texture can indeed be simplified as depicted in Fig. 4d. According to this model the bulk-like electronic structure is formed by four main bands labeled 1–4. This implies that one should always keep in mind that SARPES scans intersect these four 1–4 bands in four points denoted A-C for surface-resonances, and B-D for the bulk bands in Figs. 2b, 6 and 7.

Equally highly modulated is the out-of-plane spin-polarization $P_z$ measured at the same binding energy as MDC-B. SARPES data measured along the $\overline{\text{ΓM}}$ and $\overline{\text{ΓK}}$ directions is shown in Fig. 5a, which we relate to calculations in panel (b), with the directions denoted by blue/green arrows. The measured $P_z$ modulation shows excellent agreement with the first-principles calculations and confirms our detailed understanding of the $P_z$ warping around the Z-point, in agreement with our previous studies [25].

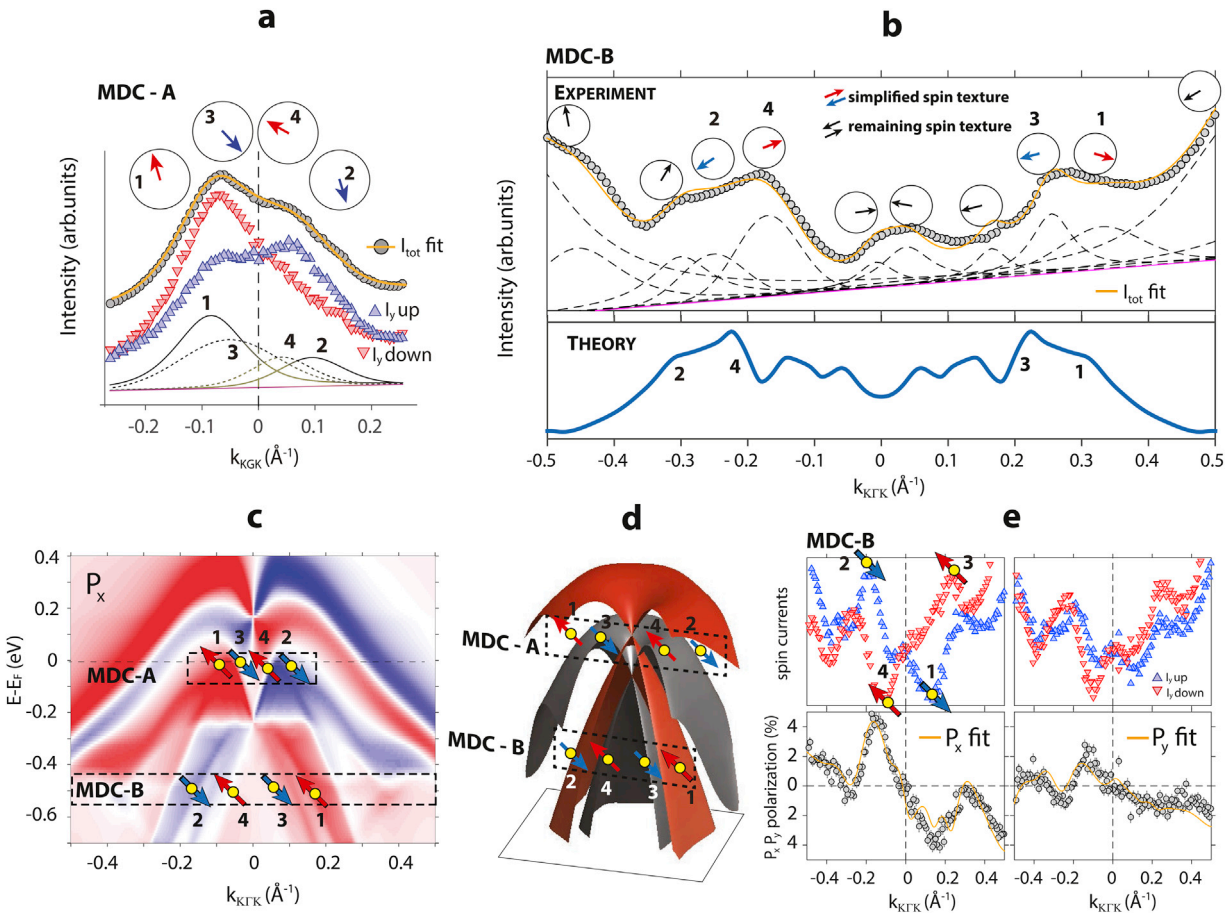


**Fig. 4.** (a) SARPES MDC measured near $E_F$ along $\overline{K\Gamma K}$ and 3D vectorial spin analysis; (b) similar at 0.5 eV binding energy. The orange line is a fit to the total photoemission intensity $I_{tot}$, the arrows above each peak (dashed lines) show the in-plane projection of the spin vector. Theoretical momentum distribution curve (blue line in bottom panel of (b)) highlights four peaks referred to as 1–4, constituting the simplified α-GeTe spin texture indicated by red/blue arrows. The remaining spin texture is denoted by black arrows. The linear background (purple dashed line) originates from the increasing inelastic background due to the changing light incidence angle. (c) $P_x$-spin component of the semi-infinite band-structure calculations in Fig. 3d with dashed rectangles indicating the resolution broadened energy ranges of MDC-A and MDC-B. (d) Simplified electronic structure model with the surface resonances in red and bulk bands in black. (e) (bottom) Measured $P_x$ and $P_y$ spin polarization and fits (orange line), and (top) derived spin currents along MDC-B. (For interpretation of the references to colour in this figure legend, the reader is referred to the web version of this article.)

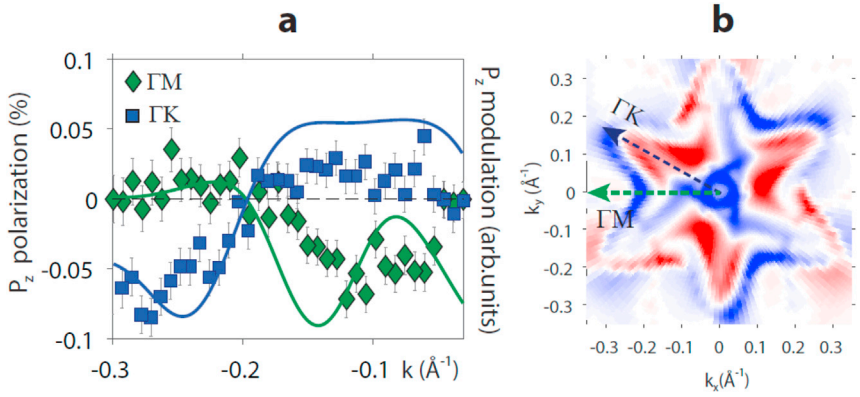


**Fig. 5.** (a) Out-of-plane spin-polarization $P_z$ measured for α-GeTe at 0.5 eV binding energy along $\overline{\Gamma M}$ and $\overline{\Gamma K}$ (symbols). Full lines show the corresponding $P_z$ modulations for the semi-infinite crystal calculations in (b).

## 4. Modification of α-GeTe by Mn-doping

Fig. 6 displays SARPES data from $Ge_{0.87}Mn_{0.13}Te$. Panels (a-c) summarize the in-plane $P_{x,y}$ spin windings above and below the Zeeman gap, and panels (d-f) summarize the out-of-plane $P_z$ spin texture around the Zeeman gap. For clarity the simplified electronic structure including magnetic order is depicted in panel (a). The Zeeman gap opens up around a binding energy of 0.1 eV. In agreement with previous studies [31], the gap size, measured in the total intensity data, is $\Delta_Z \approx 100$ meV (Fig. 6e–f).

The splitting of the surface electronic structure in B-D bulk and A-C bulk-derived surface resonance bands becomes evident in the $P_z$ spin

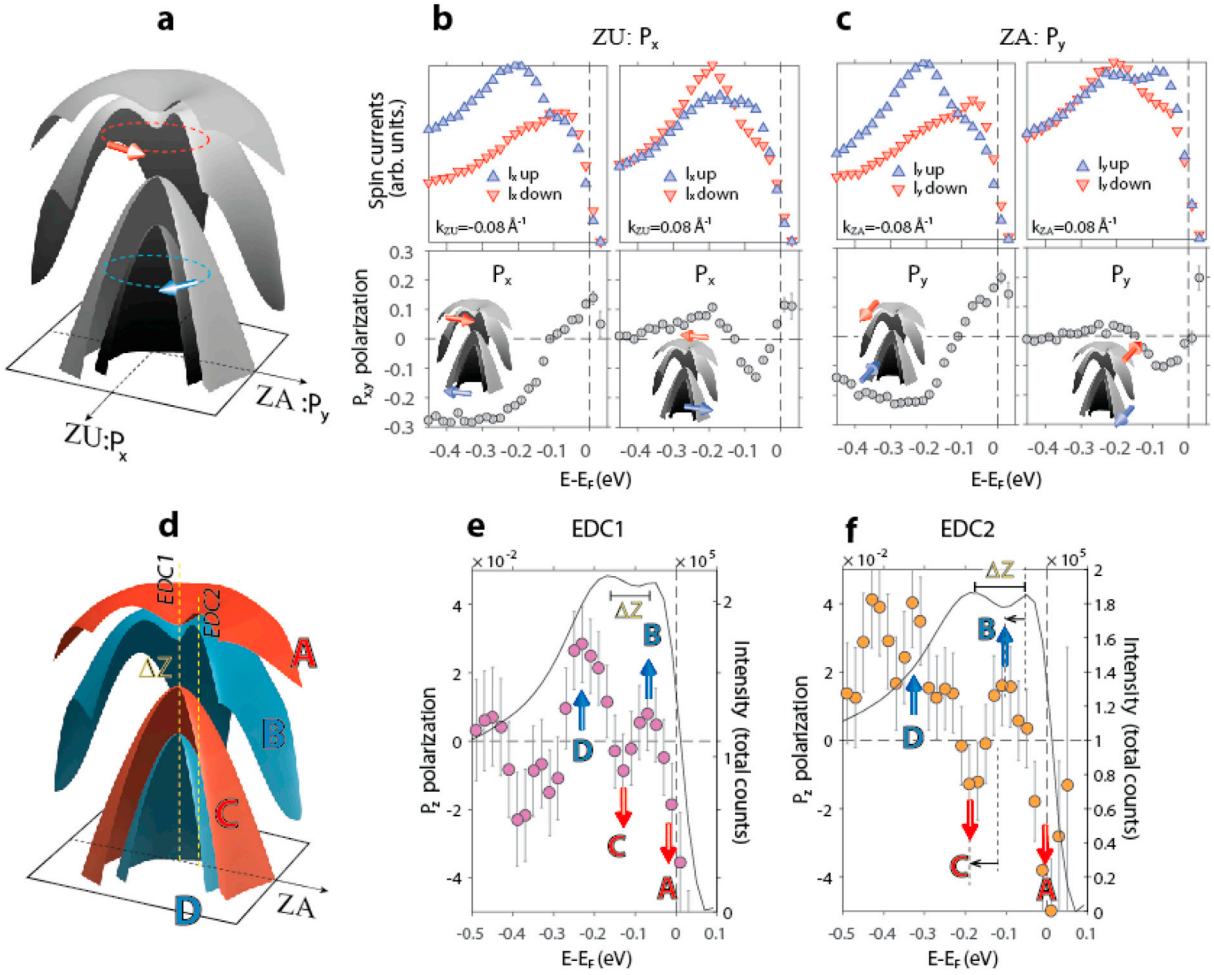


**Fig. 6.** (a) Simplified electronic structure model of the $Ge_{1-x}Mn_xTe$ bulk band structure with in-plane spin texture above and below the Zeeman gap ΔZ. (b,c) Measured $P_{x,y}$ spin polarization (bottom) and corresponding spin currents (top) for off-normal emission ($\pm 0.08 Å^{-1}$) along Z-U and Z-A directions from $Ge_{0.87}Mn_{0.13}Te$. (d) Simplified model of the out-of-plane spin texture $P_z$ from as-grown $Ge_{0.87}Mn_{0.13}Te$ samples, deduced from data measured in normal (e) and off-normal (f) emission. The red/blue arrows indicate the spin texture, the horizontal arrow in (f) indicate the shift of the bands B-C. The Zeeman gap is indicated by markers in (e,f) in the total counts (solid line). (For interpretation of the references to colour in this figure legend, the reader is referred to the web version of this article.)

texture. In order to confirm the presence of the four bands already mentioned in Fig. 2b, data are measured in normal emission (Fig. 6e) and off-normal emission (Fig. 6f), respectively. The subtle shift in binding energy of the peaks B and C indicated by horizontal arrows in panel (f), confirms the dispersion of all the bands A-D consistent with the simplified electronic structure scheme of the bulk-derived bands.

## 5. Field control of spin texture

In α-GeTe electric-field control of the spin windings is possible by placing a metallic electrode on the surface. Applying a voltage induces a change in the spin polarization. However, we find that the endurance of the spin switching caused by changing the field direction is limited due to unipolar FE fatigue and other effects such as FE domain pinning [33]. Moreover, epitaxial α-GeTe films typically display a multidomain structure [25,37,54] in which polarization reversal may involve intermediate steps via oblique domains rather than direct switching along the ⟨111⟩ axis which is coupled to the a full spin texture reversal [33].

$Ge_{1-x}Mn_xTe$ appears to have a weaker pinning of the FE polarization because the off-center displacement of the Te atom with respect to the Ge atoms in $Ge_{1-x}Mn_xTe$ decreases with increasing Mn content [37,55]. This reduces the energy barriers for switching of the atomic positions in the FE reorientation and thus leads to a softening of the FE properties while simultaneously acquiring magnetoelectric properties. Thus, from an application point of view, $Ge_{1-x}Mn_xTe$ fulfills all criteria for mutual control of magnetism and ferroelectricity via magnetoelectric coupling effects, which is a unique material property [56,57].

In order to emphasize the close relationship between α-GeTe and $Ge_{1-x}Mn_xTe$, Fig. 7 summarizes the B-field control of $Ge_{0.94}Mn_{0.06}Te$ in which the size of the Zeeman gap is less than 50 meV [31]. Data were measured at the CASSIOPÈE beamline at the Soleil synchrotron in remanent magnetization and show how the $P_z$ spin-texture from as-grown samples develops in consecutive sample magnetization cycles. Contrary to the E-field manipulation of the α-GeTe spin texture in which the spin control is basically stalled after the second cycling, the B-field control from $Ge_{0.94}Mn_{0.06}Te$ is found to change after each sample magnetization. We note that after the third magnetization cycle (Fig. 7d) the $P_z$ spin texture stabilizes in a configuration as predicted by theory for bulk $Ge_{1-x}Mn_xTe$ [31,33].

SARPES data in Figs. 6–7 confirm that apart from the Zeeman gap, the simplified surface electronic structure model of α-GeTe also applies for $Ge_{1-x}Mn_xTe$ and that manipulating the spin-texture by external fields in photoemission impart additional degrees of freedom associated with surface resonances, as seen in the gradual deployment of the $P_z$ spin-texture in Fig. 7. Our experimental observations suggest that there are certain volatile degrees of freedom in the surface electronic structure and in the spin-texture

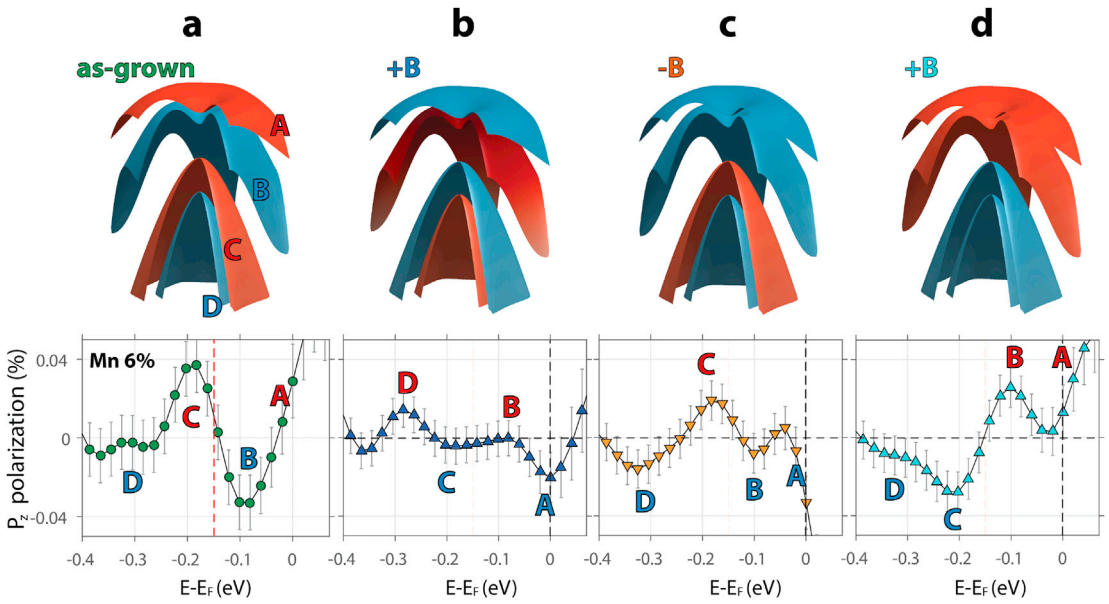


**Fig. 7.** (a–d) Deployment of the $P_z$ spin-texture of the bands A-D from $Ge_{0.94}Mn_{0.06}Te$ measured in remanent magnetization after magnetizing the sample with ±700 Gauss (see text for details).

which give rise to complex switching paths. Consequently they may result in unconventional spin texture evolutions upon manipulation by external fields [31,33] or by tuning the α-GeTe surface termination. For example the energetically less favorable α-GeTe surface termination with Ge-atoms discussed in Ref. [34] according to the simplified surface electronic structure affects only the top-most surface-resonance sheet A sitting right at $E_F$, rather than a full switching which extends to the bulk Rashba bands.

## 6. Conclusions

By comprehensive (S)ARPES mapping of the electronic structure we have evaluated in detail the spin-resolved electronic structure of the ferroelectric and multiferroic Rashba semiconductors α-GeTe and $Ge_{1-x}Mn_xTe$. The strong spin-orbit effect entails large spin splitting of the surface electronic structure consisting of surface and surface resonant states, which are shadowing the bulk Rashba bands. The different contributions can be separated and analyzed by combining measurements at different photon energies and photon polarizations. Our experimental findings are in excellent agreement with *ab-initio* calculations based on the multiple scattering approach and semi-infinite crystal calculations with included spin-orbit coupling. This leads to a simplified model of the α-GeTe and $Ge_{1-x}Mn_xTe$ surface electronic structure. Our experimental results confirm the coupling between the ferromagnetic and ferroelectric order in $Ge_{1-x}Mn_xTe$. This is the main precondition for functional spintronic applications, but presently the magneto-electric coupling imposes limited functionality due to the complex switching paths of the Rashba spin textures even at temperatures around 20 K.

## Acknowledgements

This work was supported by the Swiss National Science Foundation Project No. PP00P2_1447421 and n.200021 146890. G.S. and V.V.V. acknowledge support from the Austrian Science Funds (SFB-025, IRON). JM would like to thank CEDAMNF project (CZ.02.1.01/0.0/0.0/15_003/0000358) funded by the Ministry of Education, Youth and Sports of Czech Republic.

## References

[1] Y.A. Bychkov, E.I. Rashba, J. Phys. C Solid State Phys. 17 (1984) 6039.
[2] J. Nitta, T. Akazaki, H. Takayanagi, T. Enoki, Phys. Rev. Lett. 78 (1997) 1335.
[3] M. Maekawa (Ed.), Concepts in Spin Electronics, Oxford University Press, 2006, pp. 43–90.
[4] S. LaShell, B.A. McDougall, E. Jensen, Phys. Rev. Lett. 77 (1996) 3419.
[5] E. Rotenberg, J.W. Chung, S.D. Kevan, Phys. Rev. Lett. 82 (1999) 4066.
[6] M. Hochstrasser, J.G. Tobin, E. Rotenberg, S.D. Kevan, Phys. Rev. Lett. 89 (2002) 216802.
[7] M. Hoesch, M. Muntwiler, V.N. Petrov, M. Hengsberger, L. Patthey, M. Shi, M. Falub, T. Greber, J. Osterwalder, Phys. Rev. B 69 (2004), 241401.
[8] C.R. Ast, J. Henk, A. Ernst, L. Moreschini, M.C. Falub, D. Pacilé, P. Bruno, K. Kern, M. Grioni, Phys. Rev. Lett. 98 (2007), 186807.
[9] F. Meier, H. Dil, J. Lobo-Checa, L. Patthey, J. Osterwalder, Phys. Rev. B Condens. Matter Mater. Phys. 77 (2008), 165431.
[10] D. Hsieh, Y. Xia, L. Wray, D. Qian, A. Pal, J.H. Dil, J. Osterwalder, F. Meier, G. Bihlmayer, C.L. Kane, Y.S. Hor, R.J. Cava, M.Z. Hasan, Science 323 (2009) 919. http://www.sciencemag.org/cgi/reprint/323/5916/919.pdf.
[11] A.M. Shikin, A. Varykhalov, G.V. Prudnikova, D. Usachov, V.K. Adamchuk, Y. Yamada, J.D. Riley, O. Rader, Phys. Rev. Lett. 100 (2008), 057601.
[12] J.H. Dil, F. Meier, J. Lobo-Checa, L. Patthey, G. Bihlmayer, J. Osterwalder, Phys. Rev. Lett. 101 (2008) 266802.
[13] B. Slomski, G. Landolt, G. Bihlmayer, J. Osterwalder, J.H. Dil, Sci. Rep. 3 (2013) 1963.
[14] P.D.C. King, R.C. Hatch, M. Bianchi, R. Ovsyannikov, C. Lupulescu, G. Landolt, B. Slomski, J.H. Dil, D. Guan, J.L. Mi, E.D.L. Rienks, J. Fink, A. Lindblad, S. Svensson, S. Bao, G. Balakrishnan, B.B. Iversen, J. Osterwalder, W. Eberhardt, F. Baumberger, P. Hofmann, Phys. Rev. Lett. 107 (2011), 096802.
[15] A.F. Santander-Syro, F. Fortuna, C. Bareille, T.C. Rödel, G. Landolt, N.C. Plumb, J.H. Dil, M. Radović, Nat. Mater 13 (2014) 1085.
[16] J.H. Dil, J. Phys. Condens. Matter 21 (2009), 403001 (22pp).
[17] T. Okuda, A. Kimura, J. Phys. Soc. Jpn. 82 (2013).
[18] K. Ishizaka, M.S. Bahramy, H. Murakawa, M. Sakano, T. Shimojima, T. Sonobe, K. Koizumi, S. Shin, H. Miyahara, A. Kimura, K. Miyamoto, T. Okuda, H. Namatame, M. Taniguchi, R. Arita, N. Nagaosa, K. Kobayashi, Y. Murakami, R. Kumai, Y. Kaneko, Y. Onose, Y. Tokura, Nat. Mater 10 (2011) 521.
[19] C. Martin, E.D. Mun, H. Berger, V.S. Zapf, D.B. Tanner, Phys. Rev. B 87 (2013), 041104.
[20] G. Landolt, S.V. Eremeev, Y.M. Koroteev, B. Slomski, S. Muff, M. Kobayashi, V.N. Strocov, T. Schmitt, Z.S. Aliev, M.B. Babanly, I.R. Amiraslanov, E.V. Chulkov, J. Osterwalder, J.H. Dil, Phys. Rev. Lett. 109 (2012), 116403.
[21] J.S. Lee, G.A.H. Schober, M.S. Bahramy, H. Murakawa, Y. Onose, R. Arita, N. Nagaosa, Y. Tokura, Phys. Rev. Lett. 107 (2011), 117401.
[22] G. Landolt, S.V. Eremeev, O.E. Tereshschenko, S. Muff, B. Slomski, K.A. Kokh, M. Kobayashi, T. Schmitt, V.N. Strocov, J. Osterwalder, E.V. Chulkov, J.H. Dil, New J. Phys. 15 (2013).
[23] A. Crepaldi, L. Moreschini, G. Autés, C. Tournier-Colletta, S. Moser, N. Virk, H. Berger, P. Bugnon, Y.J. Chang, K. Kern, A. Bostwick, E. Rotenberg, O.V. Yazyev, M. Grioni, Phys. Rev. Lett. 109 (2012), 096803.
[24] D. Di Sante, P. Barone, R. Bertacco, S. Picozzi, Adv. Mater. 25 (2013) 509.
[25] J. Krempaský, H. Volfová, S. Muff, N. Pilet, G. Landolt, M. Radović, M. Shi, D. Kriegner, V. Holý, J. Braun, H. Ebert, F. Bisti, V.A. Rogalev, V.N. Strocov, G. Springholz, J. Minár, J.H. Dil, Phys. Rev. B 94 (2016), 205111.

[26] P. Fons, A.V. Kolobov, M. Krbal, J. Tominaga, K.S. Andrikopoulos, S.N. Yannopoulos, G.A. Voyiatzis, T. Uruga, Phys. Rev. B 82 (2010), 155209.
[27] M. Wuttig, D. Lusebrink, D. Wamwangi, W. Welnic, M. Gilleszen, R. Dronskowski, Nat. Mater 6 (2007) 122.
[28] L. Esaki, in: Proc. Intern. Conf. Semicond. Phys, 1966, p. 589.
[29] G.S. Pawley, W. Cochran, R.A. Cowley, G. Dolling, Phys. Rev. Lett. 17 (1966) 753.
[30] M. Liebmann, C. Rinaldi, D. Di Sante, J. Kellner, C. Pauly, R.N. Wang, J.E. Boschker, A. Giussani, S. Bertoli, M. Cantoni, L. Baldrati, M. Asa, I. Vobornik, G. Panaccione, D. Marchenko, J. Sánchez-Barriga, O. Rader, R. Calarco, S. Picozzi, R. Bertacco, M. Morgenstern, Adv. Mater. 28 (2016) 560.
[31] J. Krempaský, S. Muff, F. Bisti, M. Fanciulli, H. Volfová, A.P. Weber, N. Pilet, P. Warnicke, F. Bertran, H. Ebert, J. Braun, J. Minár, G. Springholz, J. Dil, V. Strocov, Nat. Commun. 7 (2016) 13071.
[32] H.J. Elmers, R. Wallauer, M. Liebmann, J. Kellner, M. Morgenstern, R.N. Wang, J.E. Boschker, R. Calarco, J. Sánchez-Barriga, O. Rader, D. Kutnyakhov, S.V. Chernov, K. Medjanik, C. Tusche, M. Ellguth, H. Volfova, S. Borek, J. Braun, J. Minár, H. Ebert, G. Schönhense, Phys. Rev. B94 (2016), 201403.
[33] J. Krempaský, S. Muff, J. Minár, N. Pilet, M. Fanciulli, A. Weber, V. Volobuiev, M. Gmitra, C. Vaz, V. Scagnoli, G. Springholz, J. Dil, arXiv:1707.08431v1 [cond-mat.Mtrl-sci], 2017.
[34] C.C. Rinaldi, S. Varotto, M. Asa, J. Slawinska, J. Fujii, G. Vinai, S. Cecchi, R. Calarco, I. Vobornik, G. Panaccione, S. Picozzi, B. R, arXiv:1707.07043v1 [cond-mat.Mtrl-sci], 2017.
[35] S. Picozzi, Front. Phys. 2 (2014).
[36] I.I. Klimovskikh, A.M. Shikin, M.M. Otrokov, A. Ernst, I.P. Rusinov, O.E. Tereshchenko, V.A. Golyashov, J. SÃ¡nchez-Barriga, A.Y. Varykhalov, O. Rader, K.A. Kokh, E.V. Chulkov, Sci. Rep. 7 (2017) 3353.
[37] H. Przybylińska, G. Springholz, R.T. Lechner, M. Hassan, M. Wegscheider, W. Jantsch, G. Bauer, Phys. Rev. Lett. 112 (2014), 047202.
[38] P. Stiles, L. Esaki, J. Schooley, Phys. Lett. 23 (1966) 206.
[39] V. Narayan, T.-A. Nguyen, R. Mansell, D. Ritchie, and G. Mussler, **10**, 253 (2016).
[40] C.W.J. Beenakker, Annu. Rev. Condens. Matter Phys. 4 (2013) 113.
[41] R.T. Lechner, G. Springholz, M. Hassan, H. Groiss, R. Kirchschlager, J. Stangl, N. Hrauda, G. Bauer, Appl. Phys. Lett. 97 (2010), 023101.
[42] M. Hassan, G. Springholz, R. Lechner, H. Groiss, R. Kirchschlager, G. Bauer, J. Cryst. Growth 323 (2011) 363. Proceedings of the 16th International Conference on Molecular Beam Epitaxy (ICMBE).
[43] H. Ebert, D. Ködderitzsch, J. Minár, Rep. Prog. Phys. 74 (2011).
[44] M. Hoesch, T. Greber, V.N. Petrov, M. Muntwiler, M. Hengsberger, W. Auwärter, J. Osterwalder, J. Electron Spectrosc. Relat. Phenom. 124 (2002) 263.
[45] M. Muntwiler, J. Zhang, R. Stania, F. Matsui, P. Oberta, U. Flechsig, L. Patthey, C. Quitmann, T. Glatzel, R. Widmer, E. Meyer, T.A. Jung, P. Aebi, R. Fasel, T. Greber, J. Synchrotron Radiat. 24 (2017) 354.
[46] V.N. Strocov, X. Wang, M. Shi, M. kobayashi, J. Krempaský, C. Hess, T. Schmitt, L. Patthey, J. Synchrotron Radiat. 3 (2014) 631.
[47] C.S. Fadley, Synchrotron Radiat. News 25 (2012) 26.
[48] A.H. Edwards, A.C. Pineda, P.A. Schultz, M.G. Martin, A.P. Thompson, H.P. Hjalmarson, C.J. Umrigar, Phys. Rev. B 73 (2006), 045210.
[49] M.-C. Desjonquères, D. Spanjaard, Concepts in Surface Physics, Springer, 1998.
[50] P. Yu, M. Cardona, Fundamentals of Semiconductors, Physics and Materials Properties, Springer-Verlag Berlin Heidelberg, 2010, pp. 430–490.
[51] L. Ley, M. Cardona (Eds.), Photoemission in Solids II, Springer-Verlag Berlin Heidelberg, 1979, pp. 63–67.
[52] V.N. Strocov, V.N. Petrov, J.H. Dil, J. Synchrotron Radiat. 22 (2015) 708.
[53] F. Meier, J.H. Dil, J. Osterwalder, New J. Phys. 11 (2009), 125008.
[54] R. Wang, J.E. Boschker, E. Bruyer, D.D. Sante, S. Picozzi, K. Perumal, A. Giussani, H. Riechert, R. Calarco, J. Phys. Chem. C 118 (2014) 29724.
[55] D. Kriegner, J. Furthmüller, R. Kirchschlager, J. Endres, L. Horak, P. Cejpek, H. Reichlova, X. Marti, D. Primetzhofer, A. Ney, G. Bauer, F. Bechstedt, V. Holy, G. Springholz, Phys. Rev. B 94 (2016), 054112.
[56] W. Eerenstein, N.D. Mathur, J.F. Scott, Nature 442 (2006) 759.
[57] M. Fiebig, J. Phys. D Appl. Phys. 38 (2005) R123.